



# Tropospheric ozone retrieval by a combination of TROPOMI/S5P measurements with BASCOE assimilated data

Klaus-Peter Heue<sup>1,2</sup>, Diego Loyola<sup>1</sup>, Fabian Romahn<sup>1</sup>, Walter Zimmer<sup>1</sup>, Simon Chabrilat<sup>3</sup>, Quentin Errera<sup>3</sup>, Jerry Ziemke<sup>4</sup>, and Natalya Kramarova<sup>4</sup>

<sup>1</sup>Institut für Methodik der Fernerkundung am Deutschen Zentrum für Luft- und Raumfahrt (DLR), Oberpfaffenhofen, Germany

<sup>2</sup>Technische Universität München (TUM), Munich, Germany

<sup>3</sup>Royal Belgian Institute for Space Aeronomy (BIRA-IASB), Brussels, Belgium

<sup>4</sup>NASA Goddard Space Flight Center (GSFC), Greenbelt, Maryland, USA

**Correspondence:** Klaus-Peter Heue (klaus-peter.heue@dlr.de)

Received: 14 January 2022 – Discussion started: 17 February 2022

Revised: 1 September 2022 – Accepted: 1 September 2022 – Published: 4 October 2022

**Abstract.** We present a new tropospheric ozone dataset based on TROPospheric Monitoring Instrument (TROPOMI)/Sentinel-5 Precursor (S5P) total ozone measurements combined with stratospheric ozone data from the Belgian Assimilation System for Chemical Observations (BASCOE) constrained by assimilating ozone observations from the Microwave Limb Sounder (MLS). The BASCOE stratospheric data are interpolated to the S5P observations and subtracted from the TROPOMI total ozone data. The difference is equal to the tropospheric ozone residual column from the surface up to the tropopause. The tropospheric ozone columns are retrieved at the full spatial resolution of the TROPOMI sensor ( $5.5 \times 3.5 \text{ km}^2$ ) with daily global coverage.

Compared to the Ozone Mapping and Profiler Suite Modern-Era Retrospective analysis for Research and Applications 2 (OMPS-MERRA-2) data, a global mean positive bias of 3.3 DU is found for the analysed period April 2018 to June 2020. A small negative bias of about  $-0.91$  DU is observed in the tropics relative to the operational TROPOMI tropical tropospheric data based on the convective cloud differential (CCD) algorithm throughout the same period. The new tropospheric ozone data (S5P-BASCOE) are compared to a set of globally distributed ozonesonde data integrated up to the tropopause level. We found 2254 comparisons with cloud-free TROPOMI observations within 25 km of the stations. In the global mean, S5P-BASCOE deviates by 2.6 DU from the integrated ozonesondes. Depending on the latitude

the S5P-BASCOE deviate from the sondes and between  $-4.8$  and  $7.9$  DU, indicating a good agreement. However, some exceptional larger positive deviations up to 12 DU are found, especially in the northern polar regions (north of  $70^\circ$ ). The monthly mean tropospheric column and time series for selected areas showed the expected spatial and temporal pattern, such as the wave one structure in the tropics or the seasonal cycle, including a summer maximum, in the mid-latitudes.

## 1 Introduction

Tropospheric ozone is an important pollutant because it affects human health and crop growth. Negative respiratory and cardiovascular symptoms especially increase with short-term exposure to enhanced ozone concentrations (e.g. Fleming et al., 2018). In the global mean, tropospheric ozone is responsible for a loss of about 10% of wheat production (e.g. Avery et al., 2011; Ainsworth et al., 2012) depending on the region, but crop loss may reach up to 25%. In the troposphere, ozone is produced by photo-chemical processes converting primary pollutants, such as  $\text{NO}_x$  and volatile organic compounds (VOCs), or is produced directly by lightning. Stratospheric intrusion is another important source of tropospheric ozone. Due to its long lifetime of 20 to 30 d (e.g. Wu et al., 2007), ozone can be transported over large distances. Moreover, tropospheric ozone acts as a greenhouse

gas ( $0.40 \pm 0.20 \text{ W m}^{-2}$ , IPCC, 2013) and is an important source of OH that controls the lifetime of many other atmospheric species.

Currently, several approaches are used to derive tropospheric ozone from satellite observations. In the tropics, the Convective Cloud Differential method (Ziemke et al., 1998) can be used. TROPOMI/S5P (TROPOspheric Monitoring Instrument on Sentinel 5 Precursor) tropical tropospheric ozone data (Heue et al., 2016, 2021b) have been generated operationally since December 2018 based on the convective cloud differential (CCD). The vertical ozone column above deep convective clouds gives an estimate of the stratospheric ozone column. It is assumed that the stratospheric ozone column varies slowly in time and latitude but is longitudinally constant. The stratospheric background column is averaged for a certain reference region (Indian Ocean from Indonesia to the Pacific Ocean) and subtracted from the total column for cloud-free observations.

Ziemke et al. (2006) presented a limb–nadir matching approach based on the combination of nadir observations from the Ozone Monitoring Instrument (OMI) and limb observations from the Microwave Limb Sounder (MLS), both of which are located on the NASA Aura satellite. The nadir-viewing OMI observes the total column, and MLS provides the ozone vertical distribution from 0.02 hPa down to the upper troposphere. To retrieve the stratospheric column the MLS ozone profile is assimilated to Modern-Era Retrospective analysis for Research and Applications 2 (MERRA-2, Gelaro et al., 2017) and integrated above the tropopause. Both datasets are gridded to the same grid ( $1^\circ$  latitude  $\times$   $1.25^\circ$  longitude), and only data with less than 30 % cloud coverage are considered. In addition, a version with a direct combination of OMI and MLS data is also available ([https://acd-ext.gsfc.nasa.gov/Data\\_services/cloud\\_slice/new\\_data.html](https://acd-ext.gsfc.nasa.gov/Data_services/cloud_slice/new_data.html), last access: March 2022, Ziemke et al., 2006). Both instruments are installed on the same platform and observe the same air mass within a 7 min delay. The product was further improved, and the OMI measurements were continued by OMPS (Ozone Mapping and Profiler Suite) nadir observations (Sect. 3.1.2).

SCIAMACHY (Scanning Imaging Absorption Spectrometer for Atmospheric Chartography) on Envisat (2002–2012) was capable of observing both the total column at nadir and the stratospheric profile of limb geometry. Ebojje et al. (2014) published the latest update to the limb–nadir matching data based on SCIAMACHY observations. The algorithm is in principle similar to the one used for OMI-MLS, except that the total column and the stratospheric ozone profile are both observed with the same instrument in the UV range. The limb observations are used to retrieve a stratospheric ozone profile; the profile was then integrated above the tropopause to calculate the stratospheric columns. The difference between the total column retrieved from the SCIAMACHY nadir observation and the stratospheric column results in the tropospheric residual.

Miles et al. (2015) used an optimal estimation method (Rodgers, 2000) to retrieve the profile information from GOME, SCIAMACHY, OMI, and GOME-2 nadir observations. The different sensitivities of the instruments to ozone absorption in the Hartley band and Huggins band and the temperature dependency of the ozone absorption cross section are the key parameters to retrieve the ozone profile. The data were analysed within ESA's Climate Change Initiative (CCI) project and are regularly updated for EU's Copernicus Climate Change Service (C3S). The same physical background is used by Smithsonian Astrophysical Observatory (SAO) algorithm (Huang et al., 2017) to derive ozone profiles below 60 km with 2.5 km vertical resolution from OMI observations. Since December 2021, the TROPOMI/S5P operational ozone profiles (Veeffkind et al., 2021) have been available, and these also contain tropospheric ozone subcolumns up to 6 km and from 6–12 km.

The above-mentioned ozone profiles or tropospheric data are mostly based on the ozone absorption in the UV (260 to 360 nm), with the exception of MLS. The IASI (Infrared Atmospheric Sounding Interferometer) instruments on the MetOp (A, B and C) satellites make use of the infrared ozone absorptions between wavenumbers of 1025 and 1075  $\text{cm}^{-1}$ . The FORLI (Fast Optimal Retrievals on Layers for IASI) algorithm (Boynard et al., 2018) is also based on an optimal estimation method and retrieves profiles of 39 layers up to 39 km altitude and one additional layer up to the top of atmosphere. The data are restricted to cloud coverage of less than 13 %.

A combined IASI + GOME-2 retrieval (Cuesta et al., 2013) enhances the sensitivity relative to GOME-2 or IASI, especially for the lower troposphere below 3 km. Both instruments are installed on the MetOp satellite series, and co-located spectral observations are analysed simultaneously. The final data have the same spatial resolution as IASI.

The tropospheric ozone burden can be retrieved by assimilation of both the total ozone column and the stratospheric ozone profile using chemical transfer simulations. CAMS (Copernicus Atmosphere Monitoring Service) also uses  $\text{O}_3$  total columns from TROPOMI and other satellite instruments to constrain the total ozone and MLS for the stratospheric column. Inness et al. (2019) showed that the additional assimilation of TROPOMI ozone columns improves the data quality in the tropical to mid-latitude troposphere. The CAMS ozone profiles can be downloaded at <https://ads.atmosphere.copernicus.eu/cdsapp#!/search?type=dataset> (last access: March 2022).

In this study, we introduce a new tropospheric ozone dataset, S5P-Belgian Assimilation System for Chemical Observations (BASCOE), based on TROPOMI/S5P total ozone measurements and stratospheric ozone data provided by BASCOE constrained by MLS ozone profiles. The algorithm makes use of the high spatial resolution of the TROPOMI instrument ( $5.5 \times 3.5 \text{ km}^2$ ). Sentinel 5P was launched in October 2017, and together with the future Sentinel-5 mis-

sion it will provide global measurements for decades. The BASCOE stratospheric ozone system provides a forecast of stratospheric ozone profiles. In combination with the near-real-time (NRTI) S5P total ozone columns, the tropospheric ozone column may also be provided in near real time, i.e. 3 h after sensing.

In Sect. 2, the tropospheric ozone retrieval is presented, including a brief introduction of the total ozone column algorithm and the BASCOE assimilation. In Sect. 3.1, the tropospheric ozone column datasets (OMPS-MERRA, S5P\_CCD) and ozonesonde data will be explained briefly and comparisons relative to these tropospheric ozone datasets are shown. Finally, tropospheric ozone results will be presented and briefly discussed.

## 2 Tropospheric ozone retrieval

### 2.1 S5P-BASCOE

The S5P-BASCOE tropospheric ozone retrieval is based on a three-step approach, as described in the Sects. 2.2, 2.3, and 2.4. The main inputs and intermediate data are displayed in Fig. 1. As a first step, the total ozone column is retrieved from the TROPOMI/S5P observations (Sect. 2.2); here we use the operational S5P NRTI products with a resolution of  $7 \times 3.5 \text{ km}^2$ . In the second step, the ozone profiles from BASCOE (Sect. 2.3) are integrated between the tropopause pressure and the top of the atmosphere to obtain the stratospheric column in the resolution of  $2.5^\circ \times 3.75^\circ \times 3 \text{ h}$ . In the last step, the BASCOE stratospheric column is interpolated in space and time to match the S5P observations and is subtracted from the TROPOMI total columns (Sect. 2.4).

### 2.2 TROPOMI total ozone retrieval

The Sentinel-5 Precursor (S5P) satellite was launched in October 2017 into a sun-synchronous orbit with an Equator crossing time of 13:30 UTC. TROPOMI observes the atmosphere with a daily coverage and a spatial resolution of  $5.5 \times 3.5 \text{ km}^2$  ( $7 \times 3.5 \text{ km}^2$  until 6 August 2019) and a spectral resolution of roughly 0.5 nm in the UV. The S5P near-real-time (NRTI) total ozone product is based on the well-established two-step differential optical absorption spectroscopy (DOAS) approach with an iterative air mass factor (AMF) calculation (Loyola et al., 2011; Hao et al., 2014). The slant column density is retrieved in the 325 to 335 nm wavelength range. The S5P cloud algorithm provides cloud top height, cloud optical density, and cloud fraction. The innovative approach in S5P is to treat clouds as layers of scattering droplets (Loyola et al., 2018). In addition, the same cloud model is applied for the ozone AMF calculations (Heue et al., 2021a). Garane et al. (2019) showed that the NRTI total ozone column in general agrees well with ground-based observations but shows some bias in the polar to mid-latitude winter, which was caused by the albedo climatology

(Kleipool et al., 2008) used in UPAS (Universal Processor for Atmospheric Spectrometers) version 1. To solve this problem in UPAS version 2, the surface albedo required for the AMF calculation is retrieved from the TROPOMI measurements using a full physics inverse machine learning method (Loyola et al., 2020). Currently, version 2.3.0 of UPAS is being used for generating the S5P NRTI total ozone product. Figure 1a shows an example of NRTI total column, the data are cloud filtered for further retrieval.

The presented tropospheric algorithm can be applied to the S5P vertical ozone columns retrieved with both NRTI and offline algorithm, as well as other satellites. In this paper we used total ozone products based on the UPAS version 2.1.3 of the NRTI algorithm and reprocessed internally at DLR.

### 2.3 BASCOE assimilations of ozone profiles

This implementation of BASCOE was developed to improve the representation of stratospheric composition in the EU Copernicus Atmospheric Monitoring Service (CAMS) by providing independent analyses of ozone and five other species that are also observed by MLS (HCl, ClO, HNO<sub>3</sub>, N<sub>2</sub>O, H<sub>2</sub>O). These data are used to evaluate the analyses and forecasts of stratospheric ozone that are delivered operationally by CAMS (e.g. Sudarchikova et al., 2021) and also to verify research versions of the CAMS system where the stratospheric chemistry module from the BASCOE system is implemented into the CAMS system (Huijnen et al., 2016). Since it is an operational service, the BASCOE-FD (fast delivery) system has evolved over time due to the changes in the ECMWF (European Centre for Medium-Range Weather Forecasts) operational system. Moreover, BASCOE-FD has been adapted to the updates in the MLS retrieval algorithm and those in the BASCOE system (see the change log at the following link: [http://www.copernicus-stratosphere.eu/4\\_NRT\\_products/3\\_Models\\_changelogs/BASCOE.php](http://www.copernicus-stratosphere.eu/4_NRT_products/3_Models_changelogs/BASCOE.php), last access: December 2021). BASCOE-FD operationally provides analyses of stratospheric ozone and other chemical species with a timeliness of 3–5 d in order to allow the assimilation of the Aura-MLS offline dataset. Throughout the paper BASCOE and BASCOE-FD are used as synonyms. The BASCOE-FD ozone fields are provided on a  $2.5^\circ$  latitude by  $3.75^\circ$  longitude grid with a temporal resolution of 3 h. Since March 2016, BASCOE-FD has used a vertical grid with 86 levels from the surface to 0.01 hPa. An example of the BASCOE-FD ozone mixing ratio for 16 September 2018 at 12:00 UTC between 55.19 and 51.07 hPa is shown in Fig. 1b. During this period, the Antarctic ozone hole was almost fully developed and the ozone mixing ratio above Antarctica was reduced.

An early version (q2.4) of BASCOE-FD has been evaluated against total ozone ground-based measurements, ozonesonde profiles, and satellite profiles over the period 2009–2012 (Lefever et al., 2015). The agreement was usually within  $\pm 10\%$  but degraded to  $\pm 40\%$  in the tropical

2018-09-16

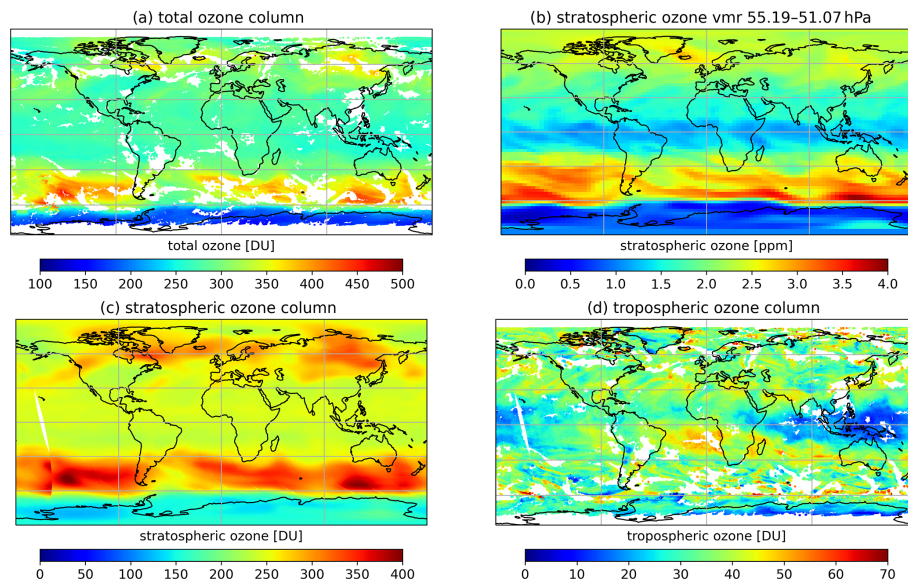


**Figure 1.** Overview of the tropospheric ozone retrieval. **(a)** TROPOMI NRTI total ozone column, where white regions represent cloud-screened data or no data availability. **(b)** BASCOE  $O_3$  mixing ratio for 16 September 2018 at 12:00 UTC around 52 hPa, with a resolution of  $2.5^\circ$  by  $3.75^\circ$ . **(c)** Integrated stratospheric ozone column from BASCOE interpolated in space and time to the TROPOMI observation; the data have the full S5P resolution, i.e.  $7 \times 3.5 \text{ km}^2$ . At  $170^\circ \text{ W}$ , the first and the last orbit of this day overlap, and thus the time difference of  $\approx 23 \text{ h}$  between these observations causes a jump in the stratospheric ozone columns. **(d)** Tropospheric ozone column calculated as the difference between the total **(a)** and stratospheric column **(c)**.

tropopause layer (TTL). The version used here (5.7) runs operationally since March 2016. It is evaluated every 3 months for the validation of the CAMS operational analyses, indicating stable biases which are usually smaller than 5% in the middle stratosphere and 15% in the TTL (e.g. Sudarchikova et al., 2021). In the upper stratosphere above 4 hPa pressure altitude, the BASCOE system has a small ozone deficit (Errera et al., 2019) that introduces a negative bias in the BASCOE-FD stratospheric ozone columns. This has been corrected using a time–latitude climatology of this bias against MLS. This climatology is based on the BASCOE-FD analyses between July 2016 and March 2019 with a resolution of  $5^\circ$  latitude and 1 d. In this work, the climatology was smoothed and linearly interpolated to  $2.5^\circ$  latitude. It varies between  $-1$  and 4 DU (Fig. 2). The integration of stratospheric columns from the BASCOE-FD analyses starts at dynamical tropopause height as given in the BASCOE-FD data files. The calculation of the tropopause pressure is done in two independent steps. First, the PV and  $\Theta$  (potential vorticity and potential temperature) tropopause is calculated. Outside the tropics (outside  $30^\circ \text{ S}$  to  $30^\circ \text{ N}$ ) the tropopause is defined as the potential vorticity isosurface at 3.5 PVU, and inside the tropics it is defined as the isentropic isosurface with a potential temperature of 380 K or 3.5 PVU (whatever is lower). The second step is based on the WMO (World Meteorological Organization) definition. The tropopause is given as the lowest altitude where the

temperature lapse rate  $dT/dz$  is less than  $2 \text{ K km}^{-1}$  and does not exceed  $2 \text{ K km}^{-1}$  in the next 2 km above. The potential vorticity and temperature are extracted from ECMWF operational analyses at a reduced spatial resolution (T31) corresponding to the coarse grid of BASCOE-FD. In the final step, the two definitions are combined by choosing the lower altitude and higher pressure level. For practical reasons, the central pressure level of the respective grid cell is given. The S5P-BASCOE data file also contains the corresponding tropopause pressures. In addition, BASCOE-FD provides data with alternative tropopause definitions, e.g. 2.5 PVU for the period from August 2019 onward. The impact of the tropopause definition on the tropospheric ozone column is discussed in Sect. 3.2.2.

## 2.4 S5P-BASCOE tropospheric ozone

The stratospheric ozone column is calculated from the BASCOE assimilated fields between the tropopause and the upper lid, i.e. 0.01 hPa. A correction term accounts for the BASCOE ozone deficit above 4 hPa. The latitude- and time-dependent climatology is added to the stratospheric ozone column, and the correction is on the order of 2 DU (Fig. 2). The stratospheric ozone column has a spatial and temporal resolution of  $3.75^\circ$  by  $2.5^\circ$  and 3 h, respectively, following the resolution of the BASCOE ozone profile.

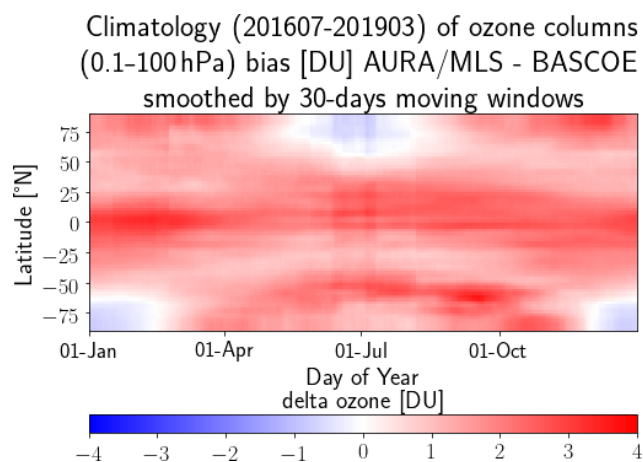


**Figure 2.** Time–latitude stratospheric ozone column bias climatology between MLS and BASCOE used to correct the BASCOE-FD stratospheric column.

**Table 1.** Mean difference and standard deviation of S5P-BASCOE relative to the individual datasets

Deviation	S5P_CCD	OMPS-MERRA-2	Sondes
DU	$-0.91 \pm 5.76$	$3.34 \pm 7.64$	$2.6 \pm 9.3$
%	$-0.82 \pm 21.71$	$14.59 \pm 32.51$	$12.8 \pm 29.1$

TROPOMI/S5P has a daily global coverage with a spatial resolution of  $5.5 \times 3.5 \text{ km}^2$ . The BASCOE stratospheric ozone column is linearly interpolated in time and space to the TROPOMI pixel centre coordinate and observation time. Figure 1c shows the interpolated stratospheric column, including the ozone deficit correction (Fig. 2). Some patterns are similar between the two subplots (1b and c); however, the interpolation and vertical integration also cause a significant smoothing. Moreover, the stratospheric column is interpolated to the TROPOMI measurement time. Note that the first and the last orbit in Fig. 1c overlap over the Pacific Ocean but differ in time by 23 h, resulting in a discontinuous ozone column.

Furthermore, the tropopause pressure as given in the BASCOE results is interpolated to the TROPOMI ground pixels and stored with the tropospheric column. Clouds shield the lower tropospheric ozone measured by satellite UV instruments. For this reason, we only take TROPOMI observations with a cloud fraction of less than 20 % for computing the tropospheric ozone. In the final step, the interpolated stratospheric column is subtracted from the total ozone column to compute the tropospheric residual; see Fig. 1d.

### 3 Comparisons to tropospheric datasets

#### 3.1 Other tropospheric ozone data

##### 3.1.1 TROPOMI\_CCD

The tropical tropospheric ozone column based on the convective cloud differential (CCD) is an official TROPOMI product generated operationally and validated regularly; the validation reports are available at <https://mpc-vdaf.tropomi.eu/index.php/search> (last access: May 2022). The algorithm has been described in a previous publication (Heue et al., 2016), and the S5P O3\_TCL ATBD (algorithm theoretical basis document) is also provided elsewhere (Heue et al., 2021b); therefore, only a short summary is given here. In a reference region ( $70^\circ \text{ E}$  to  $170^\circ \text{ W}$ ) the above-cloud column is calculated based on the TROPOMI OFFL (offline) total ozone column, based on GODFIT (GOME Direct FITting) algorithm version 4 as described in Lerot et al. (2010) and used in Inness et al. (2019). During the total column retrieval, a ghost column is added for the part of the ozone column that is shielded by clouds (inside or below the cloud). After subtracting the ghost column, the remaining column is equal to the above-cloud ozone.

The mean cloud altitude of the deep convective clouds in the reference regions is usually close to 10 km according to the TROPOMI cloud retrieval (Argyrouli et al., 2021) but varies from cloud to cloud. To normalize the above-cloud ozone column for the varying cloud altitudes to a reference level of 270 hPa, the partial ozone column between the cloud altitude and the reference level was added. This correction column is based on the climatology by McPeters and Labow (2012). For clouds higher than 10 km, we add a small correction to account for the ozone shielded between 10 km and the cloud, and for lower clouds a respective column is similarly subtracted. The above-cloud columns thereby cover the same altitude range above 10 km. In the mean the correction term is low because the mean cloud top height is close to the 10 km level. The cloud-altitude-corrected above-cloud ozone column approximates the stratospheric column. However, the real tropical tropopause is well above 10 km or 270 hPa, and the above-cloud stratospheric approximation hence also includes the upper troposphere.

It is assumed that for each latitude band the stratospheric ozone column is constant along the longitude direction and varies only slowly in time and latitude. This assumption is in general used for the CCD algorithm and is only justified within the tropics; therefore, the algorithm is limited to the latitude range between  $20^\circ \text{ S}$  and  $20^\circ \text{ N}$ . In several examples the BASCOE stratospheric column varied by less than 5 DU standard deviation within 6 d along the longitude for  $0.5^\circ$  latitude. The temporal and spatial resolution is comparable to the S5P\_CDD settings.

We subtract the stratospheric ozone column from the total ozone column for the cloud-free observations (cloud fraction

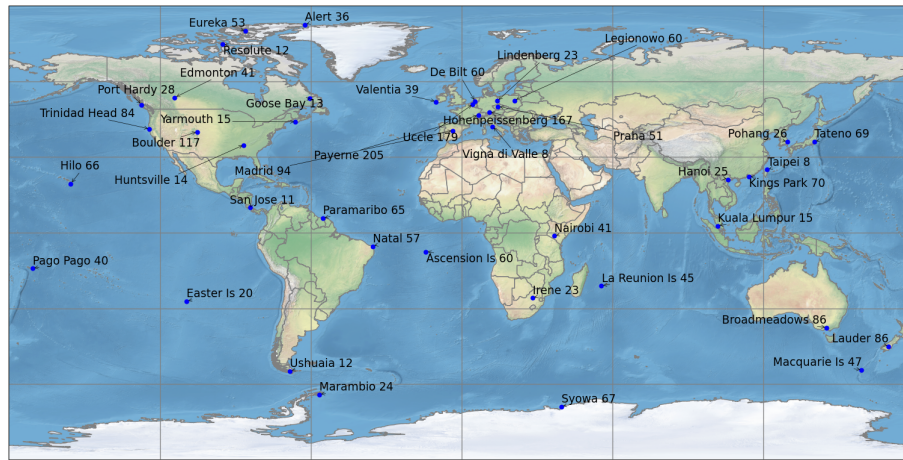


**Figure 3.** Global distribution of the ozone sounding stations. The number of soundings used in this study is given next to the station's name. Image made using Natural Earth free vector and raster map data from <https://www.naturalearthdata.com/> (last access: January 2022).

less than 10 %). The cloud-free data are averaged within a certain latitude by longitude grid and a time period. Compared to the ESA's ozone CCI tropospheric ozone, the spatial resolution was adapted to  $0.5^\circ$  latitude  $\times$   $1^\circ$  longitude. The temporal resolution for the CCI dataset from GOME-2B and OMI is 1 month, with TROPOMI it is now reduced to 6 d for the stratospheric column and 3 d for the tropospheric column. Due to the latitudinal limitations of the CCD method, the comparison between the two S5P tropospheric ozone datasets can be performed only within the tropics. The different altitude ranges from the surface to 270 hPa for CCD or to the 380 K level ( $\approx$  80 to 130 hPa) for S5P-BASCOE causes a systematic difference. For the following comparison (Sect. 3.2), we added the subcolumn between the 270 hPa reference level and 380 K based on the ozone profile by McPeters and Labow (2012).

### 3.1.2 OMPS-MERRA-2 tropospheric ozone

The evaluation of S5P-BASCOE tropospheric ozone includes comparisons with a research product of tropospheric column ozone derived by combining total column ozone from the Suomi National Polar orbiting Partnership (SNPP) Ozone Mapping Profiler Suite (OMPS) nadir mapper (NM) with stratospheric column ozone from Modern-Era Retrospective analysis for Research and Applications-2 (MERRA-2). Daily global maps of OMPS-MERRA-2 tropospheric column ozone were determined using a residual method similar to Ziemke et al. (2006) that subtracts stratospheric column ozone from total column ozone.

The OMPS-NM instrument measures total column ozone about 3 min from the TROPOMI overpass, providing an ideal dataset for cross-comparisons with TROPOMI. Total ozone from OMPS is determined using a version 2.1 algorithm that includes aerosol adjustments and cloud optical centroid pressures (OCs) retrieved from OMI. The algorithm is based on

the well-established TOMS V8 retrieval. More details on the retrieval and comparisons to other datasets are discussed in McPeters et al. (2019). The OMPS data (including quality evaluation) are available from <https://ozoneaq.gsfc.nasa.gov/data/omps/> (last access: January 2022). The OMPS-NM provides full global coverage of the sunlit Earth each day, making 400 scans per orbit with 36 across-track measurements for each scan. OMPS field of view (FOV) is about 50 km by 50 km at nadir for the 300 to 380 nm band. The MERRA-2 data assimilation system (Gelaro et al., 2017) uses Aura OMI v8.5 total ozone and MLS v4.2 stratospheric ozone profiles to produce global synoptic maps of profile ozone from the surface to the top of the atmosphere; these profiles are reported every 3 h (00:00, 03:00, 06:00 UTC, etc.) at a resolution of  $0.625^\circ$  longitude  $\times$   $0.5^\circ$  latitude. For each hourly map and at each grid point, MERRA-2 profile ozone was integrated vertically from the top of the atmosphere down to tropopause pressure to derive maps of stratospheric column ozone. Tropopause pressure was determined from MERRA-2 re-analyses using a standard PV  $\Theta$  definition (2.5 PVU and 380 K). The resulting maps of stratospheric column ozone from MERRA-2 were then co-located and subtracted from OMPS total ozone, thus producing daily global maps of tropospheric column ozone sampled at OMPS local time. These tropospheric ozone pixel measurements were binned to  $1^\circ$  latitude  $\times$   $1^\circ$  longitude resolution. In the following, the dataset will be named OMPS-MERRA-2. MERRA-2-assimilated stratosphere column ozone was found to agree within  $\pm 2$ –3 DU with the co-located MLS measurements. Comparisons between co-located ozonesonde and OMPS-MERRA-2 tropospheric column ozone in the tropics and extratropics indicate mean differences varying from near zero to at most  $\approx \pm 6$  DU, and standard deviations from a few Dobson units to at most  $\approx 6$ –8 DU (Elshorbany et al., 2021). The largest differences and standard deviations were found in the mid-latitudes and high latitudes with smaller biases in the

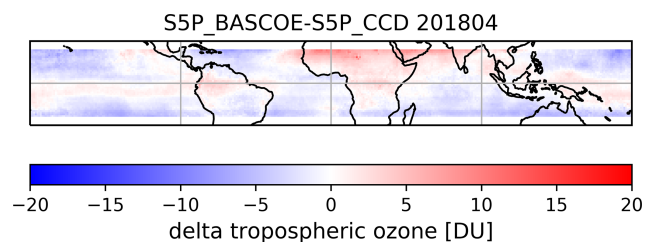


**Figure 4.** Monthly mean difference between S5P-BASCOE and S5P\_CCD for April 2018.

tropics. The OMPS-MERRA-2 tropospheric ozone columns were not filtered for clouds. There were no adjustments of any kind applied to the OMPS-MERRA-2 tropospheric column ozone.

In contrast to the CCD data, the OMPS-MERRA-2 tropospheric data provide a global dataset for the comparison. However, the analysis approach is similar to the one presented here as both use MLS data for quantifying the stratospheric contribution. Therefore, the following comparison is not based on fully independent datasets.

### 3.1.3 Ozonesondes

Ozonesondes are regularly launched from various stations around the globe. The data are provided by the respective national services and can be downloaded via World Ozone and Ultraviolet Radiation Data Centre (<https://woudc.org/data/explore.php>, last access: April 2022). The sounding stations are globally distributed. For this comparison we considered sounding data from more than 60 stations. However, some stations launch a balloon every week, while others only do so once in a month. In addition, the spatial distribution is not uniform, while nine stations in Europe provided roughly 800 soundings between 2018 and 2021, there was only one sounding station in China (Hong Kong,  $\approx 70$  soundings) and three stations were provided for the US mainland with about 220 profiles. The data distribution can be estimated from Fig. 3.

## 3.2 Comparison results

Our S5P-BASCOE tropospheric ozone data are compared to the datasets presented in Sect. 3.1. For S5P CCD (OFFL- $O_3$ ) and S5P-BASCOE (NRTI- $O_3$ ) the total ozone columns are observed with the same instrument but are retrieved using different algorithms. OMPS-MERRA-2 and S5P-BASCOE share not only the similar retrieval approach, but BASCOE and MERRA-2 both additionally assimilate MLS ozone profiles. Because of this, the satellite–satellite comparisons are not based on fully independent measurements. The ozonesondes, however, are an independent and widely accepted validation dataset. The results are described and dis-

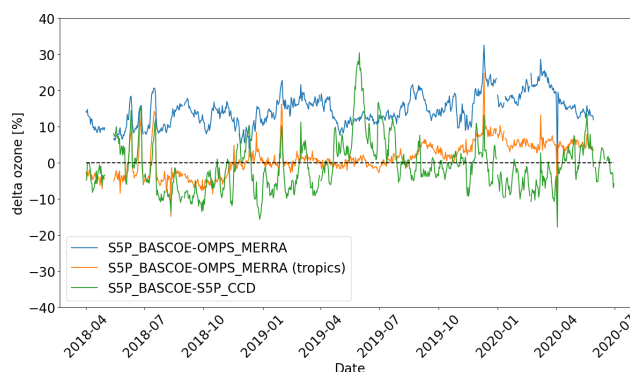


**Figure 5.** Time series of the differences between S5P-BASCOE against S5P\_CCD (green), OMPS-MERRA-2 (blue), and the tropical subset of OMPS-MERRA-2 (orange). The CCD comparison focuses on the tropical region, while for the OMPS-MERRA-2 the global datasets were also considered. In the temporal mean a negative bias ( $\approx 0.91$  DU or 0.81 %) is found relative to CCD data and a positive bias (3.34 DU or 14.59 %) is found relative to OMPS-MERRA-2.

cussed in the following sections, and a summary is given in Table 1.

Both S5P\_CCD and OMPS-MERRA-2 are gridded datasets with a resolution of  $0.5^\circ \times 1^\circ$  and  $1^\circ \times 1^\circ$  latitude by longitude, respectively. The S5P-BASCOE dataset is first gridded to  $0.25^\circ \times 0.25^\circ$  for plotting and other applications; for the comparison we averaged the grids to match the resolution of S5P\_CCD or OMPS-MLS.

### 3.2.1 Comparison to S5P\_CCD

The tropical tropospheric ozone column retrieval (S5P\_CCD) is described in Sect. 3.1.1. The data are restricted to the inner tropical range between  $20^\circ$  S and  $20^\circ$  N and include the vertical range up to 270 hPa. We use the same time period as for OMPS-MERRA-2 (Sect. 3.2.2) from April 2018 to June 2020. The CCD data were quality filtered using a minimum quality assurance (QA) value of 0.7 as recommended in Product Readme File (<https://sentinels.copernicus.eu/documents/247904/3541451>, last access: May 2022). The monthly plot for April 2018 (Fig. 4) shows that the difference is mostly negative, S5P-BASCOE is lower than S5P\_CCD, and the differences are typically less than 5 DU. There is no systematic structure like land–sea bias to be found in the plots. The time series of the tropical averaged difference between S5P-BASCOE and S5P\_CCD is illustrated in Fig. 5. The figure also includes a comparison to the OMPS-MERRA-2 tropospheric column for both the tropical subset and the global scale, which will be discussed in more detail in Sect. 3.2.2. The daily averaged tropical differences to the CCD also show a negative bias of  $-0.91$  DU and a standard variation of 5.76 DU. Three smaller peaks are observed in June and July 2018, and a large peak is observed in May and June 2019. Some of the

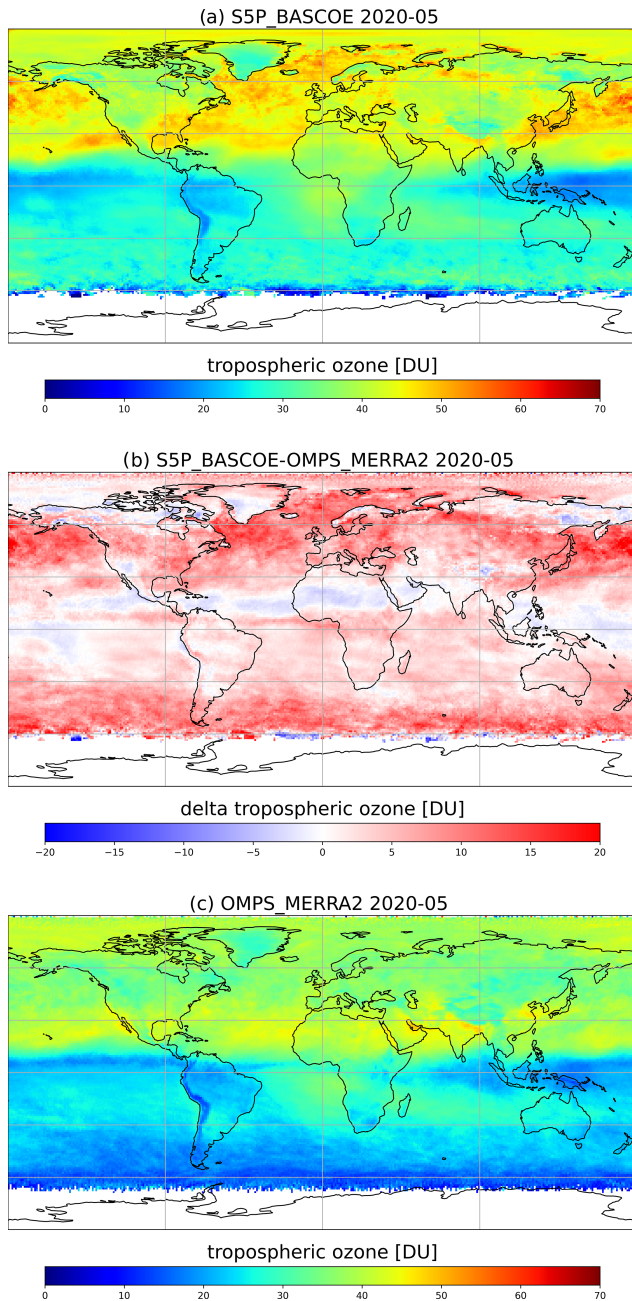


**Figure 6.** Monthly mean tropospheric ozone columns for May 2020 as observed by S5P-BASCOE (a), OMPS-MERRA-2 (c), and the difference between these two datasets (b).

peaks also occur in the comparison with OMPS-MERRA-2, especially in the tropical comparison. The large peak in May and June 2019 is not seen in the comparison to OMPS-MERRA-2, and while it results from a decrease in the S5P\_CCD data in this period, the cause is not yet fully understood. For the first peak at 10 June 2018 a deviation in the CCD data (not shown) also contributes to the increase in the differences. For the next two peaks

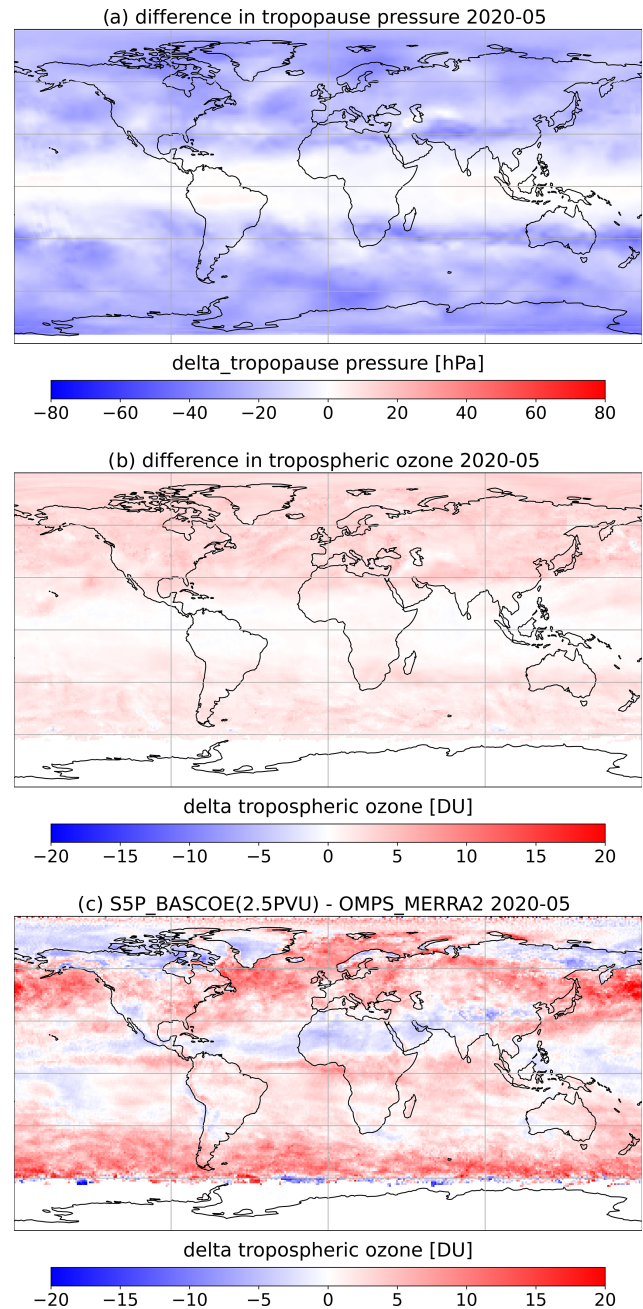


**Figure 7.** Difference in the BASCOE tropopause pressure  $P_{\text{tropopause}}(3.5 \text{ PVU}) - P_{\text{tropopause}}(2.5 \text{ PVU})$  (a) and the respective tropospheric ozone columns (b) for May 2020. Panel (c) shows the difference from OMPS-MERRA-2 (compare Fig. 6b) when using the 2.5 PVU tropopause.

there seems to be an overestimation of the tropical ozone by S5P-BASCOE. The differences to the S5P\_CCD also show a clear annual cycle, which is not seen relative to the OMPS-MERRA-2 for the global or the tropical comparison. The S5P\_CCD data probably cause the annual cycle in the difference, and this can be confirmed by an annual cycle

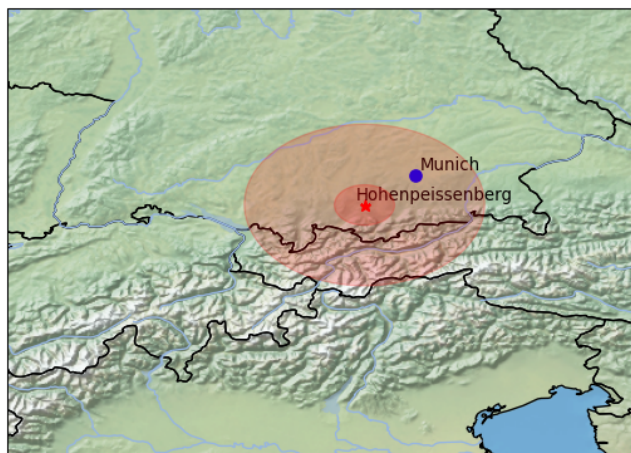


**Figure 8.** Southern Germany and the Alps, including the location of the Hohenpeißenberg sounding station and a circle of 25 km to illustrate the size of the area sampled by the satellite. For comparison, a second circle with 100 km radius is shown. The larger circle includes both urban (Munich) and alpine regions. Due to the projection the circles are slightly distorted. Image made using Natural Earth.

found in the differences with some sounding stations and GOME-2B\_CCD as documented in the validation report (<https://mpc-vdaf.tropomi.eu/index.php/search>, last access: May 2022).

### 3.2.2 Comparison to OMPS-MERRA-2

Tropospheric ozone column retrievals from OMPS-MERRA-2 are described in Sect. 3.1.2. The mean difference for May 2020 (Fig. 6) shows an underestimation around 20° N especially over the Sahara and an overestimation in the northern mid-latitudes to high latitudes and in the southern high latitudes. This pattern is also typical for the other month included in this comparison exercise. In the mean an overestimation can be found, but for large parts of the world the differences are smaller than  $\pm 5$  DU.

The globally averaged difference between S5P-BASCOE and OMPS-MERRA-2 for each day is shown in Fig. 5 together with the differences to the CCD-based tropospheric ozone. The differences vary between 2 and 6 DU with a mean difference of  $3.34 \pm 7.64$  DU. Garane et al. (2019) showed that the TROPOMI NRTI total ozone column is overestimated by  $\approx 1\%$  or 4 DU relative to Brewer and Dobson spectrometers. Compared to OMPS we can find a similar deviation in the total columns (not shown). Therefore, the deviation in the tropospheric ozone column in a similar order of magnitude is to be expected. The time series of both tropospheric ozone products S5P-BASCOE and OMPS-MERRA-2 (not shown) reveal that the three peaks in June and July 2018 are partly caused by a decrease in the OMPS-MERRA-2 dataset and to some extent by an increase in the S5P-BASCOE data. The different stratospheric ozone mod-

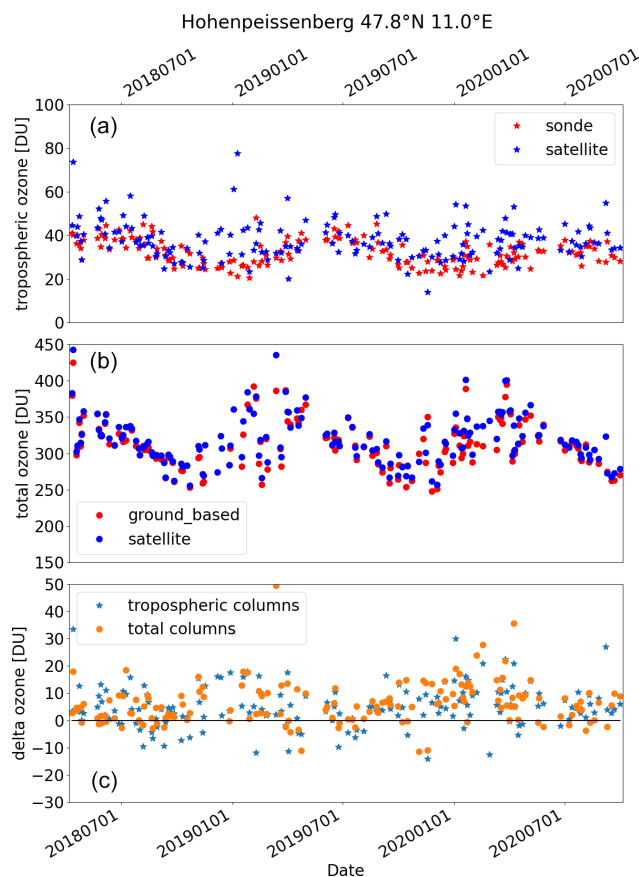


**Figure 9.** Comparison of S5P-BASCOE tropospheric ozone columns with ozonesondes at Hohenpeißenberg. In panel (a) the tropospheric columns are compared to the integrated sonde measurements. In panel (b) the total ozone columns are compared. In panel (c) the differences between the satellite data and the integrated sondes data are shown.

els BASCOE-FD (Sect. 2.3) and MERRA-2 (Sect. 3.1.2) are both constrained by MLS ozone profile observations. Nevertheless, some differences can be found. For BASCOE a small ozone deficit is known and corrected for. The correction in Fig. 2 ranges between  $-1$  and 3 DU, and in the mean it contributes 1 DU to the stratospheric column. For the tropospheric columns this causes a corresponding reduction.

The monthly mean difference between S5P-BASCOE and OMPS-MERRA-2 as shown in the centre of Fig. 6 shows a very good agreement between  $\approx 30^\circ$  N and  $30^\circ$  S. Figure 5 also confirms a better agreement in the tropics. Higher deviations occur over the northern Atlantic and Pacific up to 15 DU. Relative to the surrounding areas, the S5P-BASCOE columns increase in the regions of the maximum difference, while the OMPS-MERRA-2 data decrease in these regions (e.g. between Ireland and the central Atlantic Ocean). The size of the structures and the local changes, depending on the dataset, indicate that this might be related to cloud data. While for S5P-BASCOE the total columns are cloud filtered

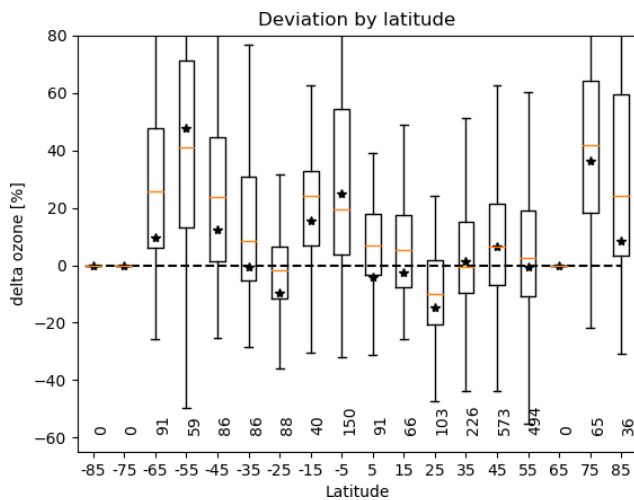


**Figure 10.** Box and whisker plot showing median deviations (red line) between S5P-BASCOE and the sonde data for 10° latitude bands and the time period between April 2018 and October 2020. The boxes represent the 25th and 75th percentile, and the stars indicate the mean deviation of the tropospheric observations closest to the stations. The number at the bottom indicates the amount of comparisons per latitude band.

and only data with cloud fractions less than 20 % are used, no cloud filter is applied during the OMPS-MERRA-2 retrieval.

In BASCOE the tropopause level is given as the lowest layer with a PV value higher than 3.5 PVU, whereas in MERRA-2 the 2.5 PVU level is used. This means that the tropopause in the S5P-BASCOE dataset is higher compared to the OMPS-MERRA-2, and hence the tropospheric column is expected to be higher. Within the tropics, where differences between the two tropospheric column datasets are smallest, both BASCOE and MERRA-2 use the 380 K potential temperature definition. For the BASCOE data after 1 August 2019 the 2.5 PVU pressure is also given in addition to standard definition. This can be used to calculate the differences caused by the different tropopause definitions, and the monthly mean for May 2020 is shown in Fig. 7. In the tropics the 380 K level is used; however, a small difference in the definitions might cause the differences in both pressure and tropospheric ozone. In BASCOE the tropopause level is given as the centre of the pressure level containing the 3.5 PVU or 380 K level, and for the comparison the 2.5 PVU/380 K pressure level is given directly. The global mean difference between these two tropospheric ozone data points equals 1.82 DU and might therefore explain the differences between our tropospheric ozone dataset and OPMS-MERRA-2 to a large extent. Moreover, the general pattern of the difference agrees well with the pattern observed in Fig. 6. Both figures show a negative deviation in the tropics and a positive one at mid-latitudes. The remaining differences (Fig. 7c) between S5P-BASCOE (2.5 PVU) and OMPS-MERRA-2 are caused either by differences in the to-

**Table 2.** Mean difference and standard deviation per 10° latitude band for the same data as displayed in Fig. 10, with the median deviation also shown.

Latitude band	Number of comparisons	Mean within 25 km radius		Standard deviation	
		%	DU	%	DU
° N					
90–80	36	32.87	8.38	42.21	10.17
80–70	65	48.44	12.07	43.60	8.75
70–60	0	–	–	–	–
60–50	494	5.83	0.35	27.36	13.43
50–40	573	10.22	2.93	26.46	8.35
40–30	226	6.34	1.25	30.98	9.18
30–20	103	−7.69	−4.84	21.59	7.99
20–10	66	6.19	1.44	19.13	5.44
10–0	91	7.75	1.71	19.25	4.67
0–−10	150	28.31	7.28	29.33	7.45
−10–−20	40	21.12	4.08	23.98	4.83
−20–−30	88	−1.11	−1.06	17.93	5.84
−30–−40	86	13.42	2.98	31.24	7.72
−40–−50	86	27.45	5.53	38.17	7.38
−50–−60	59	43.21	7.91	41.75	7.27
−60–−70	91	32.87	5.65	38.75	6.41
−70–−90	0	–	–	–	–

tal columns (1–2 DU are below 1 % of the total column) or by other differences in the stratospheric ozone columns.

### 3.2.3 Comparison to sondes

We compare the ozonesonde data for the period April 2018 to October 2020 with co-located satellite observations. We assume data to be co-located if the sounding was on the same day and the distance between the sounding station and the satellite observation was less than 25 km. The sonde data are integrated from the ground level to tropopause. The tropopause pressure (3.5 PVU) is read from the co-located S5P-BASCOE files and the mean tropopause pressure is used as upper limit for the sonde integration. We have to be aware that the surrounding may be heterogeneous with respect to urban and rural areas or mountains (Fig. 8) or sea. To reduce this effect we used a 25 km radius, for comparison 100 km is indicated in Fig. 8 as well.

Sometimes Brewer or Dobson instruments are situated next to the sounding station, and the respective total column data are provided together with the sonde profile. This allows us to compare both the total and tropospheric ozone columns. Thereby a potential deviation of the total column that might affect the tropospheric column can be detected.

For the sonde validation at Hohenpeißenberg shown in Fig. 9 an overestimation in the winter or spring season is observed. A deviation in the total columns due to the enhanced albedo in winter is already documented by Inness et al. (2019) and Garane et al. (2019). An algorithm update including a surface albedo retrieval (Loyola et al., 2020) im-

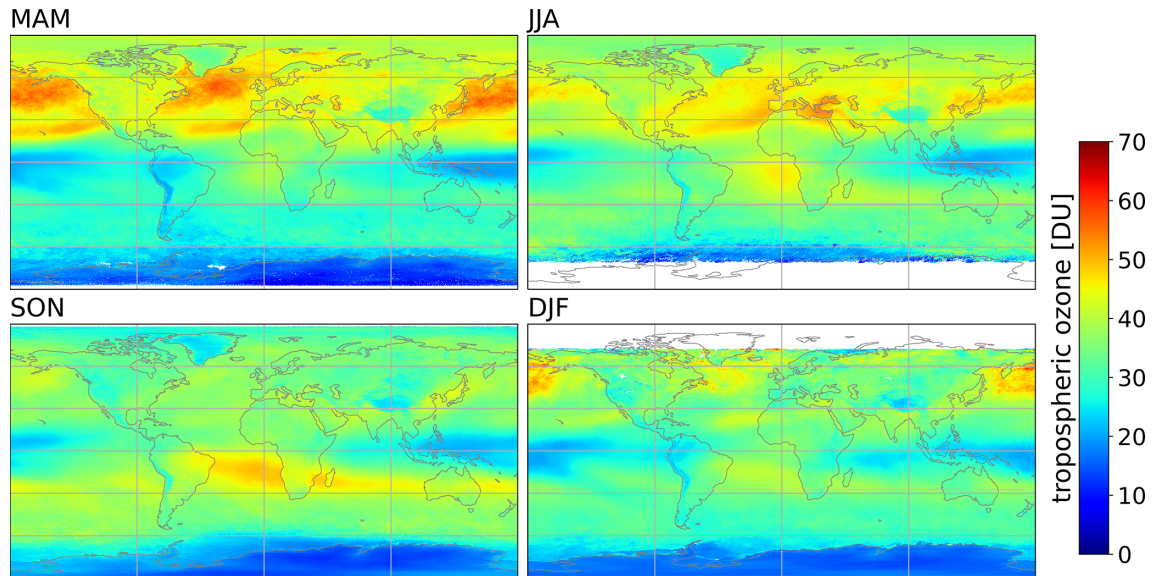


**Figure 11.** Global distribution of the mean tropospheric ozone for the four seasons obtained from S5P-BASCOE between 2018 and 2020.

proved the total columns significantly. However, a small positive bias is still observed between the TROPOMI total column and the sondes. This deviation propagates into the tropospheric column. On the other hand, there might also be an underestimation in the sonde data as Wolfgang Steinbrecht (DWD-Hohenpeißenberg) pointed out during the CEOS Atmospheric Composition Virtual Constellation Conference in June 2021. At some sonde stations the data providers integrate the data up to the top of atmosphere, assuming a climatology above the burst altitude, and compare it with nearby total column observations, e.g. from Dobson spectrometers. The measured mixing ratios are scaled according to the ratio of the total columns. This scaling is quite common but is not used in general (e.g. Logan et al., 2012). It helps harmonizing the data for long-term time series and also corrects for short-term variations and artificial drifts. The scaling factors vary between 0.8 and 1.2. However, if the ozone effective temperature is not considered in the Dobson spectrometer data retrieval, the retrieval might result in slightly smaller total ozone column, especially in the winter months. In this case the scaled sonde data is also underestimated.

The mean deviation per  $10^\circ$  latitude band (Fig. 10) also shows a small positive bias, both in the tropics and the mid-latitudes. The deviation increases towards the poles, especially for the comparison between  $70$  and  $80^\circ$  N. Similarly, for the southern polar region a systematic bias in the total ozone column was found that was partly caused by the above-mentioned albedo uncertainty. However, the bias is smaller here, and for the tropospheric ozone columns it seems to be even lower. The comparisons in the polar regions have to be taken with care, and due to the sparse sampling in time and space, the comparison is certainly not representative. A small positive bias ( $\leq 5$  DU) relative to the sonde data is found for

tropical latitudes to mid-latitudes; details are shown in Table 2. The global mean deviation equals 2.59 DU or 12.81 % with a standard deviation of 9.32 DU or 29.11 % for the 2254 comparisons used in this study. Based on the comparison, we suggest using our data mainly between  $50^\circ$  S and  $60^\circ$  N.

## 4 Results

In the previous sections we introduced a new TROPOMI/S5P tropospheric ozone product and compared it to similar satellite products and integrated ozonesondes measurements. In the following, we will discuss the tropospheric ozone columns for some specific regions.

### 4.1 Global tropospheric ozone distribution

Figure 11 shows the global tropospheric mean ozone distribution for the four seasons. All data from March, April, and May and the years 2018 to 2020 were averaged for the first subplot and each of the other plots represents an individual season as well (JJA, SON, and DJF, respectively). During the Northern Hemisphere spring the tropospheric ozone column is enhanced over the northern oceans. During the Northern Hemisphere summer three major enhancements can be seen: in the southeastern US (Sect. 4.4), eastern Mediterranean (Sect. 4.3), and northeastern China (not discussed here). In the tropics the typical wave one pattern is found throughout the year, showing a global minimum in the Pacific Ocean north of New Guinea and a maximum in the central Atlantic Ocean close to the central African coast; however, the amplitude varies with the season and is strongest from September to November. In the southern mid-latitudes no signifi-

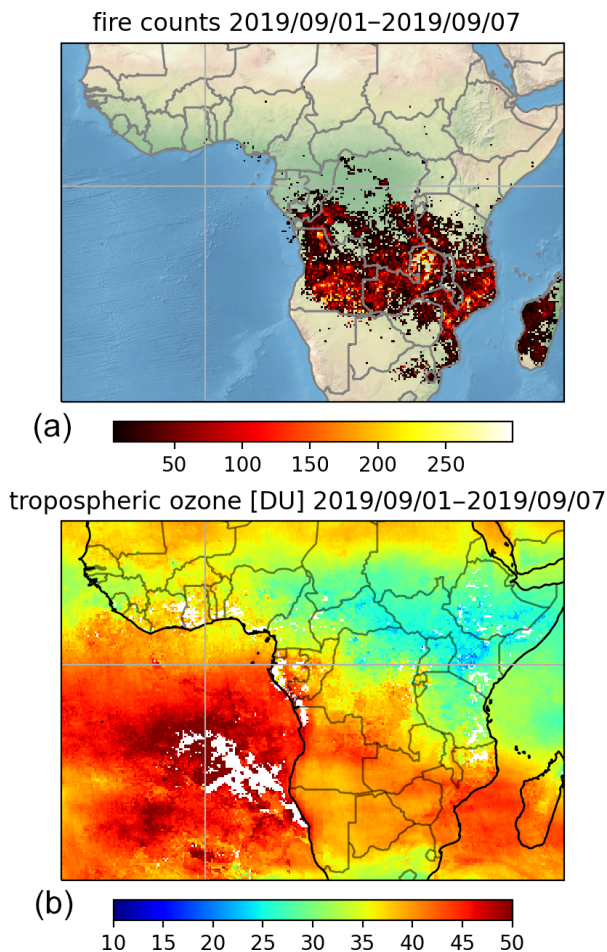


**Figure 12.** Visible Infrared Imaging Radiometer Suite (VIIRS) active fire counts for 1–7 September 2019 over Central Africa (a, image made using Natural Earth) and mean S5P-BASCOE tropospheric ozone columns for the same period (b). Fire data can be downloaded at <https://firms.modaps.eosdis.nasa.gov/download/> (last access: May 2022).

cant structure is found, and only a slight general increase in Southern Hemisphere spring is seen.

Whether the enhanced ozone columns over the northern Pacific Ocean between China, Japan, and Alaska and over the Atlantic Ocean east of the US are caused by transport or other phenomena has to be investigated in future studies. Cloud coverage and height also influence the observed tropospheric ozone pattern, as already discussed in Sect. 3.2.2. West of the Iberian peninsula over the Atlantic Ocean and west of California over the Pacific Ocean smaller transport plumes are found throughout the year with varying amplitude and latitude. The Californian plume reaches its maximum in spring, whereas the European and north African plume reaches its maximum in summer.

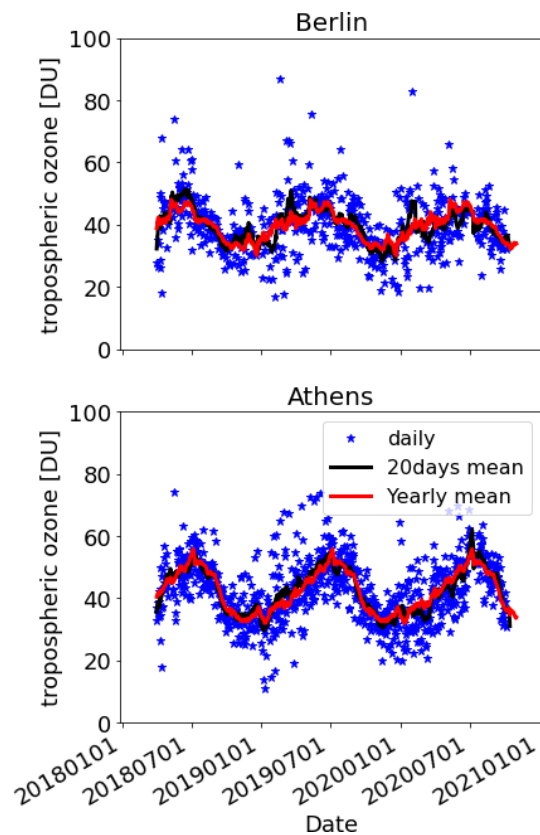


**Figure 13.** S5P-BASCOE tropospheric ozone column over Athens (Greece) and Berlin (Germany) (50 km radius around the city centre). The time series shows clear maxima in summer and minima in winter as expected. The blue stars indicate daily observations, while the black line is the 20 d running mean. For the comparison between the different years the typical annual cycle in red is included based on the 20 d running mean of each year.

## 4.2 Africa and the tropical Atlantic

Biomass burning emits both VOCs and  $\text{NO}_x$ , which are the main precursors of tropospheric ozone. Africa contributes about half of the total biomass burning carbon emissions (e.g. Pan et al., 2020). The local burning seasons move north and south following the Intertropical Convergence Zone (ITCZ), with a time shift of 6 months. The tropospheric ozone columns over the tropical Atlantic reach a maximum in the September–November season (Fig. 11). Figure 12 shows the VIIRS fire counts (<https://firms.modaps.eosdis.nasa.gov/download/>, last access: May 2022) and the respective S5p-BASCOE tropospheric ozone distribution. It is remarkable that the ozone column over the African continent is lower compared to the Atlantic Ocean. The low sensitivity of TROPOMI to ozone in the lower troposphere might cause an underestimation if the ozone concentration is enhanced close to ground. Tropospheric ozone over the tropical Atlantic is caused by combination of lightning  $\text{NO}_x$  emissions and biomass burning emission in both Africa and

North America, Ozone and Formaldehyde, 2018-07

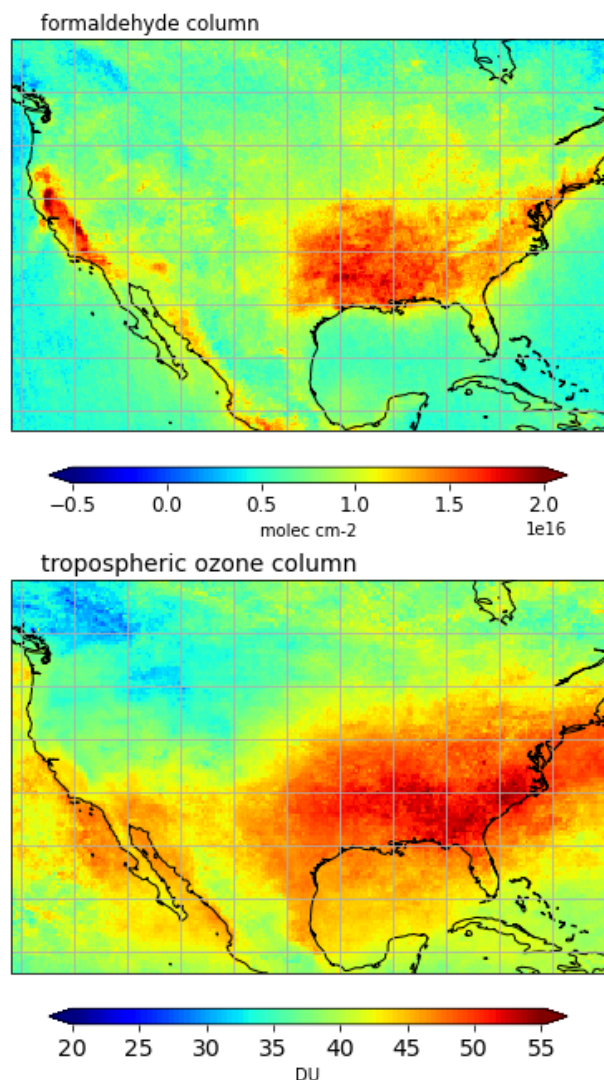


**Figure 14.** Monthly mean value of S5P formaldehyde (top) and S5P-BASCOE tropospheric ozone (bottom) over the United States observed in July 2018. Formaldehyde is a tropospheric ozone precursor.

South America combined with uplift and long-range transport. According to Moxim and Levy (2000), the polluted air masses rise over the continents and are transported over the ocean where they subside. During the transport,  $\text{NO}_x$  from lightning and biomass burning react with VOCs to ozone. Sofieva et al. (2022) included chemical transport models in their study and confirmed the enhanced columns over the Southern Atlantic in the middle troposphere. They also found low tropospheric columns over the African continent that can be attributed to the low sensitivity of UV nadir-viewing satellites for boundary layer trace gases.

### 4.3 Europe and the Mediterranean

The people living around the Eastern Mediterranean regularly suffer from high ozone concentrations in summer (e.g. Dayan et al., 2017).

The time series of tropospheric ozone columns over the Greek capital of Athens (Fig. 13) shows enhanced values for summer 2018 and 2019, reaching up to 80 DU. In July and August, several days of high column density are observed, and the lowest values are still well above 40 to 50 DU. Enhanced column density is also found throughout the years, but the column density often decreases rapidly after a few days, especially in spring. Such a decrease is hardly observed in summer. Similar time series can be found at several places around the Eastern Mediterranean, indicating stable conditions for a longer period. According to Fig. 11 the high ozone values reach from the eastern Mediterranean to the Persian Gulf. The summer 2019 was extremely dry in northern Germany and large parts of Europe, and the weather was stable for a week or 2 ([https://www.dwd.de/DE/wetter/thema\\_des\\_tages/2019/12/21.html](https://www.dwd.de/DE/wetter/thema_des_tages/2019/12/21.html), last access: January 2022). However, the time series for Berlin (Fig. 13) still shows lower tropospheric columns and a smaller amplitude in the seasonal cycle, but the day-to-day variation in the tropospheric ozone column seems higher in Berlin compared to Athens.

### 4.4 Southern United States

In the southwest of the United States high ozone columns are observed in summer. The observed tropospheric ozone columns over the United States are shown in Fig. 14. High tropospheric ozone columns are found east of  $100^\circ$  W, and this correlates very well with the enhanced formaldehyde (HCHO) columns as observed by S5P (de Smedt et al., 2018). Formaldehyde can be used as tracers for VOCs as tropospheric ozone precursors. The maximum in the tropospheric ozone is shifted to the east compared to formaldehyde. Due to the longer lifetime of ozone, the tropospheric ozone is transported to the northeast and over the Atlantic Ocean. According to sonde and airborne observations (e.g. Cooper et al., 2007), such enhancements are observed regularly in this region and are to a large extent caused by the uplift of VOC-rich air and the mixing in of lightning  $\text{NO}_x$ . A similar spatial pattern is observed over California; here the maximum of the tropospheric column is clearly separated from the HCHO enhancements.

## 5 Conclusions

We presented a new tropospheric ozone dataset based on Sentinel 5P/TROPOMI total ozone columns in combination with BASCOE stratospheric columns. The S5P-BASCOE tropospheric columns have a high TROPOMI spatial resolution of up to  $3.5 \times 5.5 \text{ km}^2$  and are in good agreement ( $3.34 \pm 7.64 \text{ DU}$ ) with the tropospheric ozone data

based on OMPS/MERRA-2. Differences in the total column and different tropopause altitude cause the observed difference. S5P\_CCD and S5P-BASCOE cover a different altitude range. For the comparison we added a correction column based on a climatology (McPeters and Labow, 2012) to the CCD data. In the mean S5P-BASCOE and S5P\_CCD the data agree very well, with a deviation of  $-0.91 \pm 5.76$  DU. The comparison shows a larger standard deviation as to OMPS-MERRA2, and at least for the current time range an annual cycle is seen. Comparison of S5P\_CCD with other datasets suggest that this might be driven by the annual cycle in the S5P\_CCD dataset. The algorithms of OMPS-MERRA-2 and S5P-BASCOE are very similar, while the S5P\_CCD data are retrieved using a completely different approach. The comparison to the ozonesondes showed a slight positive bias ( $2.6 \pm 9.3$  DU). This might be partly caused by a small overestimation in the total column data or due to an underestimation from the sondes, but the main reason is the tropospheric column itself. Relative to the sonde data, the difference increases towards the polar regions.

The S5P-BASCOE tropospheric ozone columns showed the expected global distribution. In the tropics the wave one pattern is found. During the Northern Hemisphere summer, the tropospheric ozone increases over the eastern Mediterranean or the southeastern United States. Some ozone enhancements over the Atlantic Ocean are attributed to medium-range transport.

During the COVID lockdown measures, the emissions of tropospheric ozone precursors like  $\text{NO}_x$  declined (e.g. Elshorbany et al., 2021). Due to the non-linear  $\text{NO}_x$ -VOCs-ozone chemistry the  $\text{NO}_x$  reduction does not necessarily lead to a reduction in tropospheric ozone. However, natural variability in the tropospheric ozone columns due to changes in the meteorological conditions is high. Here a longer time series of tropospheric ozone is essential to estimate natural variability, which might be on the order of the change caused by the COVID lockdown. Because of this we plan to apply the same algorithm to past and current nadir satellite ozone observations from GOME-2 and OMI. Recent studies (Thompson et al., 2021; Ziemke et al., 2019) report an increase in tropospheric ozone, and with a harmonized long-term time series these findings can be verified.

*Data availability.* Currently the S5P-BASCOE data are available on request, and we plan to set up mapping and dissemination infrastructure.

*Author contributions.* This work is only possible within a team. Klaus-Peter Heue developed the S5P tropospheric ozone algorithms presented here and prepared this paper. Diego Loyola initiated this study and supported it with numerous discussions; he also contributed to this paper through various helpful comments. Walter Zimmer and Fabian Romahn are responsible for operational UPAS

implementation of the Sentinel 5P total ozone retrieval, the CCD retrieval, and the S5P cloud retrieval. Simon Chabrilat and Quentin Errera provided the BASCOE ozone profile data and prepared the related section in the paper. Jerry Ziemke and Natalya Kramarova provided the OMPS-MERRA-2 tropospheric data, including the related section in the paper.

*Competing interests.* At least one of the (co-)authors is a member of the editorial board of *Atmospheric Measurement Techniques*. The peer-review process was guided by an independent editor, and the authors also have no other competing interests to declare.

*Disclaimer.* Publisher's note: Copernicus Publications remains neutral with regard to jurisdictional claims in published maps and institutional affiliations.

*Special issue statement.* This article is part of the special issue "Atmospheric ozone and related species in the early 2020s: latest results and trends (ACP/AMT inter-journal SI)". It is a result of the 2021 Quadrennial Ozone Symposium (QOS) held online on 3–9 October 2021.

*Acknowledgements.* Thanks to Yves Christophe (retired from BIRA-IASB) for setting up the operational process of MLS assimilation by the BASCOE system.

We gratefully acknowledge all ozonesonde data providers for providing the  $\text{O}_3$  profiles used in this paper: the WMO/GAW Ozone Monitoring Community, the World Meteorological Organization–Global Atmosphere Watch Program (WMO-GAW), and the World Ozone and Ultraviolet Radiation Data Centre (WOUDC, <https://woudc.org>, last access: December 2021). A list of all contributors is available at the following website: <https://doi.org/10.14287/10000001>. We thank NOAA for providing the ozonesonde data from Boulder, Huntsville, and Trinidad Head (<ftp://aftp.cmdl.noaa.gov/data/ozwv/Ozonesonde>, last access: March 2022).

Thanks to EU/ESA/DLR for providing the operational TROPOMI/S5P products used in this paper: total ozone, CCD tropospheric ozone, and cloud properties.

We acknowledge the use of data from NASA's Fire Information for Resource Management System (FIRMS), which is part of NASA's Earth Observing System Data and Information System (EOSDIS, <https://earthdata.nasa.gov/firms>, last access: May 2022).

The comments and suggestions provided by the reviewers and by Owen Cooper are gratefully acknowledged.

*Financial support.* This research was funded by the German Aerospace Center (DLR) in coordination with the DLR Innovative Products for Analyses of Atmospheric Composition (INPULS) project.

This work was supported by the German Research Foundation (DFG) and the Technical University of Munich (TUM) in the framework of the Open Access Publishing Program.

*Review statement.* This paper was edited by Mark Weber and reviewed by two anonymous referees.

## References

- Ainsworth, E. A., Yendrek, C. R., Sitch, S., Collins, W. J., and Embersson, L. D.: The Effects of Tropospheric Ozone on Net Primary Productivity and Implications for Climate Change, *Annu. Rev. Plant Biol.*, 63, 637–661, <https://doi.org/10.1146/annurev-arplant-042110-103829>, 2012.
- Argyrouli, A., Loyola, D., Lutz, R., and Spurr, R.: S5P/TROPOMI ATBD cloud products, S5P-DLR-L2-400I, V2.1 issue: 2.1; June 2021, available at: <https://sentinels.copernicus.eu/web/sentinel/technical-guides/sentinel-5p/products-algorithms> (last access: May 2022), 2021.
- Avnery, S., Mauzerall, D. L., Liu, J., and Horowitz, L. W.: Global crop yield reductions due to surface ozone exposure: 1. Year 2000 crop production losses and economic damage, *Atmos. Environ.*, 45, 2284–2296, <https://doi.org/10.1016/j.atmosenv.2010.11.045>, 2011.
- Boynard, A., Hurtmans, D., Garane, K., Goutail, F., Hadji-Lazaro, J., Koukouli, M. E., Wespes, C., Vigouroux, C., Keppens, A., Pommereau, J.-P., Pazmino, A., Balis, D., Loyola, D., Valks, P., Sussmann, R., Smale, D., Coheur, P.-F., and Clerbaux, C.: Validation of the IASI FORLI/EUMETSAT ozone products using satellite (GOME-2), ground-based (Brewer–Dobson, SAOZ, FTIR) and ozonesonde measurements, *Atmos. Meas. Tech.*, 11, 5125–5152, <https://doi.org/10.5194/amt-11-5125-2018>, 2018.
- Cooper, O. R., Trainer, M., Thompson, A. M., Oltmans, S. J., Tarasick, D. W., Witte, J. C., Stohl, A., Eckhardt, S., Lelieveld, J., Newchurch, M. J., Johnson, B. J., Portmann, R. W., Kalnajs, L., Dubey, M. K., Leblanc, T., McDermid, I. S., Forbes, G., Wolfe, D., Carey-Smith, T., Morris, G. A., Lefer, B., Rappenglück, B., Joseph, E., Schmidlin, F., Meagher, J., Fehsenfeld, F. C., Keating, T. J., Van Curen, R. A., and Minschwaner, K.: Evidence for a recurring eastern North America upper tropospheric ozone maximum during summer, *J. Geophys. Res.*, 112, D23304, <https://doi.org/10.1029/2007JD008710>, 2007.
- Cooper, O. R., Parrish, D. D., Ziemke, J., Balashov, N. V., Cupeiro, M., Galbally, I. E., Gilge, S., Horowitz, L., Jensen, N. R., Lamarque, J.-F., Naik, V., Oltmans, S. J., Schwab, J., Shindell, D. T., Thompson, A. M., Thouret, V., Wang, Y., and Zbinden, R. M.: Global distribution and trends of tropospheric ozone: An observation-based review, *Elem. Sci. Anth.*, 2, 000029 p., <https://doi.org/10.12952/journal.elementa.000029>, 2014.
- Cuesta, J., Eremenko, M., Liu, X., Dufour, G., Cai, Z., Höpfner, M., von Clarmann, T., Sellitto, P., Foret, G., Gaubert, B., Beekmann, M., Orphal, J., Chance, K., Spurr, R., and Flaud, J.-M.: Satellite observation of lowermost tropospheric ozone by multispectral synergism of IASI thermal infrared and GOME-2 ultraviolet measurements over Europe, *Atmos. Chem. Phys.*, 13, 9675–9693, <https://doi.org/10.5194/acp-13-9675-2013>, 2013.
- Dayan, U., Ricaud, P., Zbinden, R., and Dulac, F.: Atmospheric pollution over the eastern Mediterranean during summer – a review, *Atmos. Chem. Phys.*, 17, 13233–13263, <https://doi.org/10.5194/acp-17-13233-2017>, 2017.
- De Smedt, I., Theys, N., Yu, H., Danckaert, T., Lerot, C., Compernelle, S., Van Roozendaal, M., Richter, A., Hilboll, A., Peters, E., Pedergnana, M., Loyola, D., Beirle, S., Wagner, T., Eskes, H., van Geffen, J., Boersma, K. F., and Veeffkind, P.: Algorithm theoretical baseline for formaldehyde retrievals from S5P TROPOMI and from the QA4ECV project, *Atmos. Meas. Tech.*, 11, 2395–2426, <https://doi.org/10.5194/amt-11-2395-2018>, 2018.
- Ebojio, F., von Savigny, C., Ladstätter-Weissenmayer, A., Rozanov, A., Weber, M., Eichmann, K.-U., Bötzel, S., Rahpoe, N., Bovensmann, H., and Burrows, J. P.: Tropospheric column amount of ozone retrieved from SCIAMACHY limb–nadir-matching observations, *Atmos. Meas. Tech.*, 7, 2073–2096, <https://doi.org/10.5194/amt-7-2073-2014>, 2014.
- Elshorbany, Y. Y., Kapper, H. C., Ziemke, J. R., and Parr, S. A.: The Status of Air Quality in the United States during the COVID-19 Pandemic: A Remote Sensing Perspective, *Remote Sens.*, 13, 369, <https://doi.org/10.3390/rs13030369>, 2021.
- Errera, Q., Chabrillat, S., Christophe, Y., Deboscher, J., Hubert, D., Lahoz, W., Santee, M. L., Shiotani, M., Skachko, S., von Clarmann, T., and Walker, K.: Technical note: Reanalysis of Aura MLS chemical observations, *Atmos. Chem. Phys.*, 19, 13647–13679, <https://doi.org/10.5194/acp-19-13647-2019>, 2019.
- Fleming, Z. L., Doherty, R. M., von Schneidmesser, E., Malley, C. S., Cooper, O. R., Pinto, J. P., Colette, A., Xu, X., Simpson, D., Schultz, M. G., Lefohn, A. S., Hamad, S., Moolla, R., Solberg, S., and Feng, Z.: Tropospheric Ozone Assessment Report: Present-day ozone distribution and trends relevant to human health, *Elem. Sci. Anth.*, 6, 12, <https://doi.org/10.1525/elementa.273>, 2018.
- Garane, K., Koukouli, M.-E., Verhoelst, T., Lerot, C., Heue, K.-P., Fioletov, V., Balis, D., Bais, A., Bazureau, A., Dehn, A., Goutail, F., Granville, J., Griffin, D., Hubert, D., Keppens, A., Lambert, J.-C., Loyola, D., McLinden, C., Pazmino, A., Pommereau, J.-P., Redondas, A., Romahn, F., Valks, P., Van Roozendaal, M., Xu, J., Zehner, C., Zerefos, C., and Zimmer, W.: TROPOMI/S5P total ozone column data: global ground-based validation and consistency with other satellite missions, *Atmos. Meas. Tech.*, 12, 5263–5287, <https://doi.org/10.5194/amt-12-5263-2019>, 2019.
- Gaudel, A., Cooper, O. R., Ancellet, G., Barret, B., Boynard, A., Burrows, J. P., Clerbaux, C., Coheur, P.-F., Cuesta, J., Cuevas, E., Doniki, S., Dufour, G., Ebojio, F., Foret, G., Garcia, O., Granados-Muñoz, M. J., Hannigan, J., Hase, F., Hassler, B., Huang, G., Hurtmans, D., Jaffe, D., Jones, N., Kalabokas, P., Kerridge, B., Kulawik, S., Latter, B., Leblanc, T., Le Flochmoën, E., Lin, W., Liu, J., Liu, X., Mahieu, E., McClure-Begley, A., Neu, J., Osman, M., Palm, M., Petetin, H., Petropavlovskikh, I., Querel, R., Rahpoe, N., Rozanov, A., Schultz, M. G., Schwab, J., Siddans, R., Smale, D., Steinbacher, M., Tanimoto, H., Tarasick, D., Thouret, V., Thompson, A. M., Trickl, T., Weatherhead, E., Wespes, C., Worden, H., Vigouroux, C., Xu, X., Zeng, G., and Ziemke, J.: Tropospheric Ozone Assessment Report: Present-day distribution and trends of tropospheric ozone relevant to climate and global atmospheric chemistry model evaluation, *Elem. Sci. Anth.*, 6, 39, <https://doi.org/10.1525/elementa.291>, 2018.
- Gelaro, R., McCarty, W., Suárez, M. J., Todling, R., Molod, A., Takacs, L., Randles, C. A., Darmenov, A., Bosilovich, M. G., Reichle, R., Wargan, K., Coy, L., Cullather, R., Draper, C., Akella, S., Buchard, V., Conaty, A., da Silva, A. M., Gu, W., Kim, G., Koster, R., Lucchesi, R., Merkova, D., Nielsen, J. E., Partyka, G., Pawson, S., Putman, W., Rienecker, M., Schubert, S. D., Sienkiewicz, M., and Zhao, B.: The Modern-Era Retrospective

- Analysis for Research and Applications, Version 2 (MERRA-2), *J. Climate*, 30, 5419–5454, <https://doi.org/10.1175/JCLI-D-16-0758.1>, 2017.
- Hao, N., Koukouli, M. E., Inness, A., Valks, P., Loyola, D. G., Zimmer, W., Balis, D. S., Zyrichidou, I., Van Roozendaal, M., Lerot, C., and Spurr, R. J. D.: GOME-2 total ozone columns from MetOp-A/MetOp-B and assimilation in the MACC system, *Atmos. Meas. Tech.*, 7, 2937–2951, <https://doi.org/10.5194/amt-7-2937-2014>, 2014.
- Heue, K.-P., Coldewey-Egbers, M., Delcloo, A., Lerot, C., Loyola, D., Valks, P., and van Roozendaal, M.: Trends of tropical tropospheric ozone from 20 years of European satellite measurements and perspectives for the Sentinel-5 Precursor, *Atmos. Meas. Tech.*, 9, 5037–5051, <https://doi.org/10.5194/amt-9-5037-2016>, 2016.
- Heue, K.-P., Spurr, R., Loyola, D., Van Roozendaal, M., Lerot, C., and Xu, J.: ATBD for Total Ozone Column, S5P-L2-DLR-ATBD-400A, V2.3, issue 2.1, June, available at: <https://sentinels.copernicus.eu/web/sentinel/technical-guides/sentinel-5p/products-algorithms> (last access: May 2022), 2021a.
- Heue, K.-P., Eichmann, K.-U., and Valks, P.: ATBD for Tropospheric Ozone Column, S5P-L2-DLR-ATBD-400C, V2.3, issue 2.3, June, available at: <https://sentinels.copernicus.eu/web/sentinel/technical-guides/sentinel-5p/products-algorithms> (last access: May 2022), 2021b.
- Huang, G., Liu, X., Chance, K., Yang, K., Bhartia, P. K., Cai, Z., Allaart, M., Ancellet, G., Calpini, B., Coetzee, G. J. R., Cuevas-Agulló, E., Cupeiro, M., De Backer, H., Dubey, M. K., Fuentetaja, H. E., Fujiwara, M., Godin-Beekmann, S., Hall, T. J., Johnson, B., Joseph, E., Kivi, R., Kois, B., Komala, N., König-Langlo, G., Laneve, G., Leblanc, T., Marchand, M., Minschwaner, K. R., Morris, G., Newchurch, M. J., Ogino, S.-Y., Ohkawara, N., Piders, A. J. M., Posny, F., Querel, R., Scheele, R., Schmidlin, F. J., Schnell, R. C., Schrems, O., Selkirk, H., Shiotani, M., Skrivánková, P., Stübi, R., Taha, G., Tarasick, D. W., Thompson, A. M., Thouret, V., Tully, M. B., Van Malderen, R., Vömel, H., von der Gathen, P., Witte, J. C., and Yela, M.: Validation of 10-year SAO OMI Ozone Profile (PROFOZ) product using ozonesonde observations, *Atmos. Meas. Tech.*, 10, 2455–2475, <https://doi.org/10.5194/amt-10-2455-2017>, 2017.
- Huijnen, V., Flemming, J., Chabrillat, S., Errera, Q., Christophe, Y., Blechschmidt, A.-M., Richter, A., and Eskes, H.: C-IFS-CB05-BASCOE: stratospheric chemistry in the Integrated Forecasting System of ECMWF, *Geosci. Model Dev.*, 9, 3071–3091, <https://doi.org/10.5194/gmd-9-3071-2016>, 2016.
- Inness, A., Flemming, J., Heue, K.-P., Lerot, C., Loyola, D., Ribas, R., Valks, P., van Roozendaal, M., Xu, J., and Zimmer, W.: Monitoring and assimilation tests with TROPOMI data in the CAMS system: near-real-time total column ozone, *Atmos. Chem. Phys.*, 19, 3939–3962, <https://doi.org/10.5194/acp-19-3939-2019>, 2019.
- IPCC: Climate Change 2013: The Physical Science Basis, in: Contribution of Working Group I to the Fifth Assessment Report of the Intergovernmental Panel on Climate Change, edited by: Stocker, T. F., Qin, D., Plattner, G.-K., Tignor, M., Allen, S. K., Boschung, J., Nauels, A., Xia, Y., Bex, V., and Midgley, P. M., 1535, Cambridge University Press, Cambridge, United Kingdom and New York, NY, USA, 2013.
- Kleipool, Q. L., Dobber, M. R., de Haan, J. F., and Levett, P. F.: Earth surface reflectance climatology from 3 years of OMI data, *J. Geophys. Res.*, 113, D18308, <https://doi.org/10.1029/2008JD010290>, 2008.
- Lefever, K., van der A, R., Baier, F., Christophe, Y., Errera, Q., Eskes, H., Flemming, J., Inness, A., Jones, L., Lambert, J.-C., Langerock, B., Schultz, M. G., Stein, O., Wagner, A., and Chabrillat, S.: Copernicus stratospheric ozone service, 2009–2012: validation, system intercomparison and roles of input data sets, *Atmos. Chem. Phys.*, 15, 2269–2293, <https://doi.org/10.5194/acp-15-2269-2015>, 2015.
- Lerot, C., Van Roozendaal, M., Lambert, J.-C., Granville, J., van Gent, J., Loyola, D., and Spurr, R.: The GODFIT algorithm: a direct fitting approach to improve the accuracy of total ozone measurements from GOME, *Int. J. Remote Sens.*, 31, 543–550, <https://doi.org/10.1080/01431160902893576>, 2010.
- Logan, J. A., Staehelin, J., Megretskaia, I. A., Cammas, J.-P., Thouret, V., Claude, H., De Backer, H., Steinbacher, M., Scheel, H.-E., Stübi, R., Fröhlich, M., and Derwent, R.: Changes in ozone over Europe: Analysis of ozone measurements from sondes, regular aircraft (MOZAIC) and alpine surface sites, *J. Geophys. Res.*, 117, D09301, <https://doi.org/10.1029/2011JD016952>, 2012.
- Loyola, D., Koukouli, M. E., Valks, P., Balis, D. S., Hao, N., Van Roozendaal, M., Spurr, R. J. D., Zimmer, W., Kiemel, S., Lerot, C., and Lambert, J.-C.: The GOME-2 total column ozone product: Retrieval algorithm and ground-based validation, *J. Geophys. Res.*, 116, D07302, <https://doi.org/10.1029/2010JD014675>, 2011.
- Loyola, D. G., Gimeno García, S., Lutz, R., Argyrouli, A., Romahn, F., Spurr, R. J. D., Pedergnana, M., Doicu, A., Molina García, V., and Schüssler, O.: The operational cloud retrieval algorithms from TROPOMI on board Sentinel-5 Precursor, *Atmos. Meas. Tech.*, 11, 409–427, <https://doi.org/10.5194/amt-11-409-2018>, 2018.
- Loyola, D. G., Xu, J., Heue, K.-P., and Zimmer, W.: Applying FP\_ILM to the retrieval of geometry-dependent effective Lambertian equivalent reflectivity (GE\_LER) daily maps from UVN satellite measurements, *Atmos. Meas. Tech.*, 13, 985–999, <https://doi.org/10.5194/amt-13-985-2020>, 2020.
- McPeters, R. D. and Labow, G. J.: Climatology 2011: An MLS and sonde derived ozone climatology for satellite retrieval algorithms, *J. Geophys. Res.*, 117, D10303, <https://doi.org/10.1029/2011JD017006>, 2012.
- McPeters, R., Frith, S., Kramarova, N., Ziemke, J., and Labow, G.: Trend quality ozone from NPP OMPS: the version 2 processing, *Atmos. Meas. Tech.*, 12, 977–985, <https://doi.org/10.5194/amt-12-977-2019>, 2019.
- Miles, G. M., Siddans, R., Kerridge, B. J., Latter, B. G., and Richards, N. A. D.: Tropospheric ozone and ozone profiles retrieved from GOME-2 and their validation, *Atmos. Meas. Tech.*, 8, 385–398, <https://doi.org/10.5194/amt-8-385-2015>, 2015.
- Moxim, W. and Levy II, H.: A model analysis of the tropical South Atlantic ocean tropospheric ozone maximum: the interaction of transport and chemistry, *J. Geophys. Res.*, 105, 393e17,415, <https://doi.org/10.1029/2000JD900175>, 2000.
- Pan, X., Ichoku, C., Chin, M., Bian, H., Darmenov, A., Colarco, P., Ellison, L., Kucsera, T., da Silva, A., Wang, J., Oda, T., and Cui, G.: Six global biomass burning emission datasets: inter-

- comparison and application in one global aerosol model, *Atmos. Chem. Phys.*, 20, 969–994, <https://doi.org/10.5194/acp-20-969-2020>, 2020.
- Rodgers, C.: Inverse methods for atmospheric sounding: theory and practice, series on atmospheric, oceanic and planetary physics, Vol. 2, Singapore, New Jersey, London, Hong Kong: World Scientific, <https://doi.org/10.1142/3171>, 2000.
- Sofieva, V. F., Hänninen, R., Sofiev, M., Szeląg, M., Lee, H. S., Tamminen, J., and Retscher, C.: Synergy of Using Nadir and Limb Instruments for Tropospheric Ozone Monitoring (SUNLIT), *Atmos. Meas. Tech.*, 15, 3193–3212, <https://doi.org/10.5194/amt-15-3193-2022>, 2022.
- Sudarchikova, N., Schulz, M., Errera, Q., Ramonet, M., Eskes, H. J., Basart, S., Benedictow, A., Bennouna, Y., Blechschmidt, A.-M., Chabrilat, S., Christophe, Y., Cuevas, E., El-Yazidi, A., Flentje, H., Fritzsche, P., Hansen, K. M., Im, U., Kapsomenakis, J., Langerock, B., Richter, A., Thouret, V., Wagner, A., Warneke, T., and Zerefos, C.: Validation report of the CAMS near-real-time global atmospheric composition service: Period September–November 2020, Copernicus Atmosphere Monitoring Service (CAMS) report, <https://doi.org/10.24380/rysv-7371>, March 2021.
- Thompson, A. M., Stauffer, R. M., Wargan, K., Witte, J. C., Kollonige, D. E., and Ziemke, J. R.: Regional and seasonal trends in tropical ozone from SHADOZ profiles: Reference for models and satellite products, *J. Geophys. Res.-Atmos.*, 126, e2021JD034691, <https://doi.org/10.1029/2021JD034691>, 2021.
- Veefkind, P., Keppens, A., and de Haan, J.: ATBD for Ozone Profile, S5P-KNMI-L2-0004-RP, V1.0, Issue 1.0, October, <https://sentinels.copernicus.eu/web/sentinel/technical-guides/sentinel-5p/products-algorithms> (last access: May 2022), 2021.
- Wu, S., Mickley, L. J., Jacob, D. J., Logan, J. A., Yantosca, R. M., and Rind, D.: Why are there large differences between models in global budgets of tropospheric ozone?, *J. Geophys. Res.*, 112, D05302, <https://doi.org/10.1029/2006JD007801>, 2007.
- Ziemke, J. R., Chandra, S., and Bhartia, P. K.: Two new methods for deriving tropospheric column ozone from TOMS measurements: The assimilated UARS MLS/HALOE and convective-cloud differential techniques, *J. Geophys. Res.*, 103, 22115–22127, <https://doi.org/10.1029/98JD01567>, 1998.
- Ziemke, J. R., Chandra, S., Duncan, B. N., Froidevaux, L., Bhartia, P. K., Levelt, P. F., and Waters, J. W.: Tropospheric ozone determined from Aura OMI and MLS: Evaluation of measurements and comparison with the Global Modeling Initiative's Chemical Transport Model, *J. Geophys. Res.*, 111, D19303, <https://doi.org/10.1029/2006JD007089>, 2006.
- Ziemke, J. R., Oman, L. D., Strode, S. A., Douglass, A. R., Olsen, M. A., McPeters, R. D., Bhartia, P. K., Froidevaux, L., Labow, G. J., Witte, J. C., Thompson, A. M., Haffner, D. P., Kramarova, N. A., Frith, S. M., Huang, L.-K., Jaross, G. R., Seftor, C. J., Deland, M. T., and Taylor, S. L.: Trends in global tropospheric ozone inferred from a composite record of TOMS/OMI/MLS/OMPS satellite measurements and the MERRA-2 GMI simulation, *Atmos. Chem. Phys.*, 19, 3257–3269, <https://doi.org/10.5194/acp-19-3257-2019>, 2019.